Extended Synaptotagmin Localizes to Presynaptic ER and Promotes Neurotransmission and Synaptic Growth in *Drosophila*

Koto Kikuma,*,† Xiling Li,*,† Daniel Kim,* David Sutter,* and Dion K. Dickman*,[1]
*Department of Neurobiology and †Neuroscience Graduate Program, University of Southern California, Los Angeles, California 90089

ABSTRACT The endoplasmic reticulum (ER) is an extensive organelle in neurons with important roles at synapses including the regulation of cytosolic Ca^{2+}, neurotransmission, lipid metabolism, and membrane trafficking. Despite intriguing evidence for these crucial functions, how the presynaptic ER influences synaptic physiology remains enigmatic. To gain insight into this question, we have generated and characterized mutations in the single *extended synaptotagmin* (*Esyt*) ortholog in *Drosophila melanogaster*. Esyts are evolutionarily conserved ER proteins with Ca^{2+}-sensing domains that have recently been shown to orchestrate membrane tethering and lipid exchange between the ER and plasma membrane. We first demonstrate that Esyt localizes to presynaptic ER structures at the neuromuscular junction. Next, we show that synaptic growth, structure, and homeostatic plasticity are surprisingly unperturbed at synapses lacking *Esyt* expression. However, neurotransmission is reduced in *Esyt* mutants, consistent with a presynaptic role in promoting neurotransmitter release. Finally, neuronal overexpression of *Esyt* enhances synaptic growth and the sustainment of the vesicle pool during intense activity, suggesting that increased Esyt levels may modulate the membrane trafficking and/or resting Ca^{2+} pathways that control synapse extension. Thus, we identify *Esyt* as a presynaptic ER protein that can promote neurotransmission and synaptic growth, revealing the first *in vivo* neuronal functions of this conserved gene family.

KEYWORDS *Drosophila*; neuromuscular junction; endoplasmic reticulum; synapse

THE endoplasmic reticulum (ER) is an essential intracellular organelle present across metazoans with critical but enigmatic roles at synapses. The importance of the synaptic ER is underscored by its involvement in human disease, including hereditary spastic paraplegias (Blackstone *et al.* 2011; Montenegro *et al.* 2012; Noreau *et al.* 2014), amyotrophic lateral sclerosis (Teuling *et al.* 2007; Yang *et al.* 2009; Fasana *et al.* 2010), and Alzheimer's disease (Cheung *et al.* 2008; Zhang *et al.* 2009; Goussakov *et al.* 2010). At presynaptic terminals, the ER has significant roles in both membrane trafficking and the local regulation of Ca^{2+} signaling (Verkhratsky 2005; Chakroborty *et al.* 2009; Renvoisé and Blackstone 2010; Deng *et al.* 2013; Kwon *et al.* 2016). In particular, the ER can modulate constitutive membrane trafficking pathways to the plasma membrane that are necessary for proper synaptic growth and maintenance (Pfenninger 2009; Ramirez and Couve 2011; Deng *et al.* 2013; Deshpande and Rodal 2016). In addition, the presynaptic ER tightly regulates local Ca^{2+} dynamics by orchestrating intracellular Ca^{2+} release and sequestration (Bardo *et al.* 2006; Chakroborty *et al.* 2009; Kwon *et al.* 2016; de Juan-Sanz *et al.* 2017). However, the molecules and mechanisms through which the presynaptic ER controls synaptic growth and function remain obscure.

Extended synaptotagmins (Esyts) are a family of ER-resident proteins that are attractive candidates to function as modulators of synaptic growth and activity. Esyts are defined by the presence of a hydrophobic stretch (HS) followed by a synaptotagmin-like mitochondrial lipid-binding protein (SMP) domain and multiple Ca^{2+}-binding C_2 domains (Min *et al.* 2007; Giordano *et al.* 2013). Esyt is evolutionarily conserved from yeast (Tricalbin, Tcb1–3) through mammals (Esyt1–3) (Min *et al.* 2007; Manford *et al.* 2012; Herdman and Moss 2016), suggesting this gene family performs important functions that have

doi: https://doi.org/10.1534/genetics.117.300261
Manuscript received May 23, 2017; accepted for publication September 1, 2017; published Early Online September 7, 2017.
Supplemental material is available online at www.genetics.org/lookup/suppl/doi:10.1534/genetics.117.300261/-/DC1.
[1]Corresponding author: HNB 309, Department of Neurobiology, University of Southern California, 3641 Watt Way, Los Angeles, CA 90089. E-mail: dickman@usc.edu

been selected for and maintained throughout evolution. Studies in yeast and mammalian cell culture have revealed that Esyts mediate tethering of ER–plasma membrane (PM) contact sites to facilitate ER–PM lipid transfer (Giordano *et al.* 2013; Saheki *et al.* 2016; Yu *et al.* 2016; Saheki and De Camilli 2017), while other functions for Esyts have also been proposed (Jean *et al.* 2010, 2012; Tremblay *et al.* 2015). Interestingly, Esyt-dependent membrane tethering and lipid transfer is activated only upon relatively high intracellular concentrations of Ca^{2+}, such as those achieved during store-operated Ca^{2+} entry and neurotransmission (Idevall-Hagren *et al.* 2015). This raises the intriguing possibility that Esyt may become active in modulating lipid metabolism during synaptic activity. However, a recent study reported no apparent changes in synaptic function in mutant mice lacking all three *Esyt* isoforms (Sclip *et al.* 2016), leaving open questions about what functions, if any, Esyts may have at synapses.

The fruit fly *Drosophila melanogaster* is a powerful model system to elucidate the *in vivo* functions of *Esyt*. In contrast to mammals, there is a single, highly conserved *Esyt* ortholog. Further, the fly neuromuscular junction (NMJ) enables an array of imaging, electrophysiological, and genetic approaches to illuminate the fundamental roles of genes at synapses. We have therefore generated and characterized the first *Esyt* mutations in *Drosophila* to test the role of *Esyt* in synaptic growth, function, and plasticity. Specifically, we examined synapses lacking and overexpressing *Esyt* at basal states and under synaptic stress. These studies have defined a role for *Esyt* at the presynaptic ER in promoting neurotransmission and synaptic growth.

Materials and Methods

Fly stocks

All *Drosophila* stocks were raised at 25° on standard molasses food. The w^{1118} strain was used as the wild-type control unless otherwise noted, as this was the genetic background into which all genotypes and transgenic lines were crossed. The *Drosophila* stocks used in this study were the following: *OK6-Gal4* (Aberle *et al.* 2002), *BG57-Gal4* (Budnik *et al.* 1996), *UAS-GFP-KDEL* (Dong *et al.* 2013; Nandi *et al.* 2014), *UAS-GFP-myc-2xFYVE* (Wucherpfennig *et al.* 2003), and *UAS-PLCδ1-PH-GFP* (Verstreken *et al.* 2009; Khuong *et al.* 2010). The $Esyt^2$ mutant ($Mi\{ET1\}Esyt2^{MB029221}$), the deficiency [$Df(3R)Exel7357$], and all other stocks were obtained from the Bloomington *Drosophila* Stock Center unless otherwise noted. Female larvae were used unless otherwise specified. Phylogenetic analysis was performed using PhyML 3.0 software (Guindon *et al.* 2010), and visualized using FigTree software (http://tree.bio.ed.ac.uk/software/figtree/).

Molecular biology

There are four predicted *Esyt* isoforms in *Drosophila* based on expressed sequence tags (http://flybase.org/reports/FBgn0266758.html). However, one transcript, *Esyt2-RB*, appears to be the major isoform based on expression profiling. Therefore, we generated transgenic *Esyt* constructs using the *Esyt2-RB* transcript (RE26910; BDGP). Full-length *Esyt* complementary DNA was PCR amplified and subcloned into the pACU2 vector (Han *et al.* 2011). An mCherry or 3xFlag tag was inserted in frame into the C-terminal end of the pACU2-*Esyt* construct. To generate the mCherry-tagged Esyt construct lacking the HS domain ($Esyt^{\Delta HS}$), the *Drosophila Esyt* HS was identified by the SMART domain online tool (http://smart.embl-heidelberg.de/). *Esyt* coding DNA before and after the identified HS were separately PCR amplified and ligated into the pACU2-*mCherry* vector using the Gibson Assembly Cloning Kit (E5510S; New England Biolabs, Beverly, MA). Finally, to generate pACU2-$Esyt^{D\text{-}N}$, the conserved aspartates in each C_2 domain were identified and mutated into asparagine (D364N, D374N, D421N, D423N, E429Q for C_2A; D517N, D564N for C_2B; D746N, D752N for C_2C). All constructs were inserted into the VK18 recombination site on the second chromosome by BestGene (Chino Hill, CA).

$Esyt^1$ mutants were generated using a CRISPR/Cas9 genome editing strategy as described (Gratz *et al.* 2013). Briefly, a target Cas9 cleavage site in *Esyt* was chosen in the earliest target of the first common exon shared by all putative *Esyt* isoforms without obvious off-target sequences in the *Drosophila* genome [single-guide RNA (sgRNA) target sequence: 5′-GACAAATGGAAACTCAATTGTGG-3′, PAM underscored]. DNA sequences covering this target sequence were synthesized and subcloned into the pU6-BbsI-chiRNA plasmid (45946; Addgene). To generate the sgRNA, pU6-BbsI-chiRNA was PCR amplified and cloned into the pattB vector (Bischof *et al.* 2007). This construct was injected and inserted into the VK18 target sequence and balanced. Screening of 20 lines with active CRISPR mutagenesis led to 17 independent deletions or insertions with predicted frameshift mutations in the *Esyt* open reading frame. The line which produced the earliest stop codon (K32stop) was chosen for further analyses and named the $Esyt^1$ allele.

Immunohistochemistry

Wandering third-instar larvae were dissected in ice-cold 0 Ca^{2+}-modified HL3 saline (Stewart *et al.* 1994; Dickman *et al.* 2005) containing 70 mM NaCl, 5 mM KCl, 10 mM $MgCl_2$, 10 mM $NaHCO_3$, 115 mM sucrose, 5 mM trehelose, 5 mM HEPES, pH 7.2, and immunostained as described (Chen *et al.* 2017). Briefly, larvae were washed three times with modified HL3 saline, and fixed in either Bouin's fixative (HT10132-1L; Sigma Chemical, St. Louis, MO) or 4% paraformaldehyde in PBS (F8775; Sigma Chemical). Larvae were washed with PBS containing 0.1% Triton X-100 (PBST) and incubated in primary antibodies at 4° overnight. The larvae were then washed in PBST and incubated in secondary antibodies at room temperature for 2 hr. Samples were transferred in VectaShield (Vector Laboratories, Burlingame, CA) and mounted on glass cover slides. The following antibodies were used: mouse anti-Bruchpilot [BRP, nc82, 1:100;

Developmental Studies Hybridoma Bank (DSHB)], affinity-purified rabbit anti-GluRIII [1:2000 (Marrus *et al.* 2004; Chen *et al.* 2017)], mouse anti-Flag (1:500, F1804; Sigma-Aldrich), guinea pig anti-vGlut [1:2000 (Chen *et al.* 2017)], mouse anti-FasII (1:20, 1D4; DSHB), and mouse anti-GFP (1:1000, 3e6; Invitrogen, Carlsbad, CA). Alexa Fluor 647-conjugated goat anti-HRP (Jackson ImmunoResearch) was used at 1:200. Donkey anti-mouse, anti-rabbit, and anti-guinea pig Alexa Fluor 488, Cy3, and Rhodamine Red X secondary antibodies (Jackson ImmunoResearch) were used at 1:400.

Confocal imaging and analysis

Larval muscle 4 of abdominal segments A2 and A3 were imaged on a Nikon (Garden City, NY) A1R resonant scanning confocal microscope using a 100× APO 1.4 NA oil immersion objective with NIS-Elements software as described (Chen *et al.* 2017). The fluorescence signals were excited by separate channels with laser lines of 488, 561, and 637 nm. Images were acquired using identical settings optimized for signal detection without saturation for all genotypes within an experiment. The general analysis tool kit in the NIS-Elements software was used to quantify bouton number, BRP and GluRIII puncta number, and density by applying intensity thresholds on each of the three channels. For live imaging of $Esyt^{mCh}$, third-instar larvae were dissected, washed, and incubated in Alexa Fluor 647-conjugated goat anti-HRP in 0 Ca^{2+}-modified HL3 at 1:200 for 5 min. The samples were then washed in 0 Ca^{2+} saline and mounted on glass cover slides. Images were acquired and analyzed as described above.

FM1-43 experiments were performed as described (Dickman *et al.* 2005). Briefly, larvae were dissected in ice-cold 0 Ca^{2+}-modified HL3 and washed, then stimulated for 10 min with a modified HL3 solution containing 90 mM KCl and 10 μM FM1-43 (Molecular Probes, Eugene, OR). Larvae were then washed in 0 Ca^{2+} saline before imaging. Images were acquired using a Nikon A1R confocal microscope using a 60× APO 1.0 NA water immersion objective and imaged as described above. The general analysis tool kit in the NIS-Elements software was used to quantify the mean intensity by applying intensity thresholds.

Western blotting

Third-instar larval CNS extracts (50 animals of each genotype) and adult heads (seven of each genotype) were homogenized in ice-cold lysis buffer (10 mM HEPES and 150 mM NaCl, pH 7.4), mixed with an EDTA-free protease inhibitor cocktail (Roche), and run on 4–12% Bis Tris Plus Gels (Invitrogen). After blotting onto PVDF membrane (Novex, Encinitas, CA) and incubation with 5% nonfat milk in TBST (10 mM Tris, pH 8.0, 150 mM NaCl, 0.5% Tween 20) for 60 min, the membrane was washed once with TBST and incubated with anti-Esyt (1:2000) and anti-actin (1:2000, JLA20; DSHB) antibodies overnight at 4°. Membranes were washed and incubated with a 1:5000 dilution of HRP-conjugated secondary antibodies (Jackson ImmunoResearch) for 1 hr. Blots were washed with TBST and developed with the ECL Plus Western Blotting System (HyGLO). To generate Esyt polyclonal antibodies, a peptide antigen was synthesized consisting of amino acids 799–816 of Esyt (CTQTGLNSWFDLQPEIRHE). This peptide was conjugated to KLH and injected into two rabbits (Cocalico, Lancaster County, PA). The rabbit immunosera was affinity purified and used at 1:2000.

Electron microscopy

Electron-microscopy analysis was performed as described (Atwood *et al.* 1993). Wandering third-instar larvae were dissected in Ca^{2+}-free HL3, then fixed in 2.5% glutaraldehyde/0.1 M cacodylate buffer at 4°. Larvae were then washed in 0.1 M cacodylate buffer. The whole mount body wall musculature was placed in 1% osmium tetroxide/0.1 M cacodylate buffer at room temperature for 1 hr. After washing, larvae were then dehydrated in ethanol. Samples were cleared in propylene oxide and infiltrated with 50% Eponate 12 in propylene oxide overnight. The following day, samples were embedded in fresh Eponate 12. Electron micrographs were obtained on a Morgagni 268 Transmission Electron Microscope (FEI, Hillsboro, OR). The junctional region was serially sectioned at a thickness of 60–70 nm. Sections were stained in 2% uranyl acetate for 3 min, washed briefly 3× in distilled water, stained in Reynolds lead citrate for 1 min, washed briefly 3× in distilled water, and dried. Sections were mounted on Formvar-coated single slot grids. Larval muscles 6/7 of abdominal segments were viewed at 23,000× magnification and acquired with a Megaview II CCD camera. Images were analyzed blind to genotype using the general analysis tool kit in the NIS-Elements software.

Electrophysiology

All dissections and recordings were performed in modified HL3 saline at room temperature with 0.4 mM $CaCl_2$ (unless otherwise specified). Sharp electrode two-electrode voltage clamp recordings (electrode resistance between 10 and 35 MΩ) were performed on muscles 6 of abdominal segments A2 and A3 as described (Kiragasi *et al.* 2017). Briefly, recordings were acquired using an Axoclamp 900A Amplifier, Digidata 1440A acquisition system, and pClamp 10.5 software (Molecular Devices). Electrophysiological sweeps were digitized at 10 kHz, and filtered at 1 kHz. Miniature excitatory postsynaptic currents (mEPSCs) were recorded for 1 min in the absence of any stimulation. Excitatory postsynaptic currents (EPSCs) were recorded while cut motor axons were stimulated for a 0.5-msec duration using an ISO-Flex Stimulus Isolator (A.M.P.I.). Intensity was adjusted for each cell, in such a way as to consistently elicit responses from both neurons innervating the muscle segment, but avoiding overstimulation. In all voltage clamp recordings, muscles were clamped at −70 mV. Recordings were rejected when muscle input resistance was <3 MΩ, or leak current >10 nA. Data were analyzed using Clampfit (Molecular Devices), MiniAnalysis (Synaptosoft), Excel (Microsoft, Redmond, WA),

and SigmaPlot (Systat) software. Average mEPSC, EPSC, and quantal content were calculated for each genotype. Larvae with intact motor nerves were dissected and incubated with or without 20 μM philanthotoxin-433 (PhTx-433) (Sigma Chemical) for 10 min to block postsynaptic glutamate receptors as described (Frank *et al.* 2006; Dickman and Davis 2009).

Statistical analysis

All data are presented as mean ± SEM. Data were compared using either a one-way ANOVA and tested for significance using a two-tailed Bonferroni *post hoc* test or a Student's *t*-test (where specified) with Graphpad Prism or Microsoft Excel software, and with varying levels of significance assessed as * $P < 0.05$, ** $P < 0.01$, *** $P < 0.001$, and ns, not significant. Quantal content was calculated for each individual recording using the equation QC = EPSC/mEPSC. Full statistical details and information can be found in Supplemental Material, Table S1.

Data availability

Fly stocks are available upon request and can be obtained from the Bloomington Stock Center. Table S1 lists the genotypes used and full statistical details for each figure.

Results

Generation of null mutations in Drosophila Esyt

The yeast and rodent genomes encode three *Esyt* isoforms [*Esyt1*, *Esyt2*, and *Esyt3* (Min *et al.* 2007; Manford *et al.* 2012)]. In contrast, the *Drosophila* genome encodes a single *Esyt* ortholog, closest and equally similar to the three mouse *Esyts* by phylogeny analyses (Figure 1, A and B). RNA-sequencing data suggests that *Esyt* is expressed in the embryonic stages after 10 hr through adulthood in all tissues examined (Daines *et al.* 2011; Graveley *et al.* 2011; Berger *et al.* 2012), consistent with *Esyt* being ubiquitously expressed. We generated a null mutation in the *Drosophila Esyt* gene, $Esyt^{1}$, using CRISPR/Cas9 genome editing technology (Gratz *et al.* 2013). $Esyt^{1}$ encodes a frameshift mutation predicted to generate a stop codon at position 32, truncating the Esyt protein before the HS (Figure 1, C and D). In addition, we obtained a separate *Esyt* mutation ($Esyt^{2}$) containing a Minos-mediated integration cassette (MiMIC) transposon insertion in the first coding intron. This transposon has a gene trap cassette (Venken *et al.* 2011; Nagarkar-Jaiswal *et al.* 2015) that is predicted to truncate the *Esyt* transcript by introducing a stop codon at the second amino acid (Figure 1, C and D). We generated a polyclonal antibody against a C-terminal stretch of the *Drosophila* Esyt protein, which recognized an immunoblot band at ~90 kDa (Figure 1, E and F), consistent with the predicted molecular mass of Esyt. Using this antibody, we confirmed that Esyt is expressed in the adult brain and larval CNS, and that $Esyt^{1}$ and $Esyt^{2}$ are protein null mutations by immunoblot analysis (Figure 1, E and F). These *Esyt* mutants are viable and fertile. Finally, we generated a series of transgenic *Esyt* constructs under *UAS* control (Figure 1D). We engineered a full-length *Esyt* transgene tagged with both mCherry and 3xFlag tags ($Esyt^{mCh}$), and a separate transgene tagged with only a 3xFlag tag ($Esyt^{Flag}$). We also generated an *Esyt* transgene without the conserved HS ($Esyt^{\Delta HS}$), which is predicted to disrupt membrane targeting of Esyt (Giordano *et al.* 2013), and specifically mutated each C_2 domain to render them unable to bind to Ca^{2+} ($Esyt^{D\text{-}N}$; see *Materials and Methods*). Using these reagents, we went on to determine the presynaptic localization of Esyt.

The HS anchors Esyt to axonal ER

In neurons, the ER is an extensive network present in the somatic perinucleus as well as in distal dendrites and axons (Summerville *et al.* 2016; de Juan-Sanz *et al.* 2017). Given that ER proteins can have uniform or heterogeneous localization in the elaborate ER network (Chang and Liou 2016), we sought to determine the subcellular localization of *Drosophila* Esyt at presynaptic terminals. We were unable to obtain specific immunolabeling against endogenous Esyt using the antibody we generated. We also attempted to generate an endogenously tagged Esyt using recombinase-mediated cassette exchange with the MiMIC insertion in the *Esyt* locus, but this effort was unsuccessful. Therefore, we expressed tagged *Esyt* constructs in motor neurons. $Esyt^{mCh}$ trafficked to presynaptic terminals, where it colocalized with an established ER marker, and the ER retention signal KDEL fused to GFP (*GFP-KDEL*; Figure 2A; Okajima *et al.* 2008).

Next, we tested whether Esyt localization and trafficking to the ER was dependent on the HS domain and on Ca^{2+} binding to the C_2 domains. Previous studies have shown that the HS domain tethers Esyt to the ER, while deletion of the HS domain shifts Esyt localization to the cytosol and PM (Min *et al.* 2007; Giordano *et al.* 2013). We therefore expressed $Esyt^{\Delta HS}$ in neurons (see Figure 1D and *Materials and Methods*). As expected, the $Esyt^{\Delta HS}$ signal was no longer restricted to the axonal ER, and instead filled the presynaptic terminal, indicating a shift to cytosolic localization (Figure 2B). We then tested the requirement of Ca^{2+} binding for Esyt trafficking and localization by expressing $Esyt^{D\text{-}N}$, which lacks the negatively charged amino acids in each C_2 domain required for Ca^{2+} binding. Interestingly, we were unable to detect any $Esyt^{D\text{-}N}$ signal at synaptic terminals (Figure 2, C and D). Instead, most of the $Esyt^{D\text{-}N}$ signal was restricted to the cell body (data not shown). This indicates that trafficking of Esyt to synaptic terminals requires the ability to bind Ca^{2+}, although we cannot exclude the possibility that the D-N mutations might have resulted in misfolding of the protein, potentially disrupting trafficking or stability. We also found that expression of $Esyt^{D\text{-}N}$ led to embryonic lethality when driven pan-neuronally or in muscle. This is not unexpected, as others have observed that synaptotagmin expression with similar mutations to C_2 domains acquired a lethal toxicity (Mackler *et al.* 2002). Together, these data demonstrate that

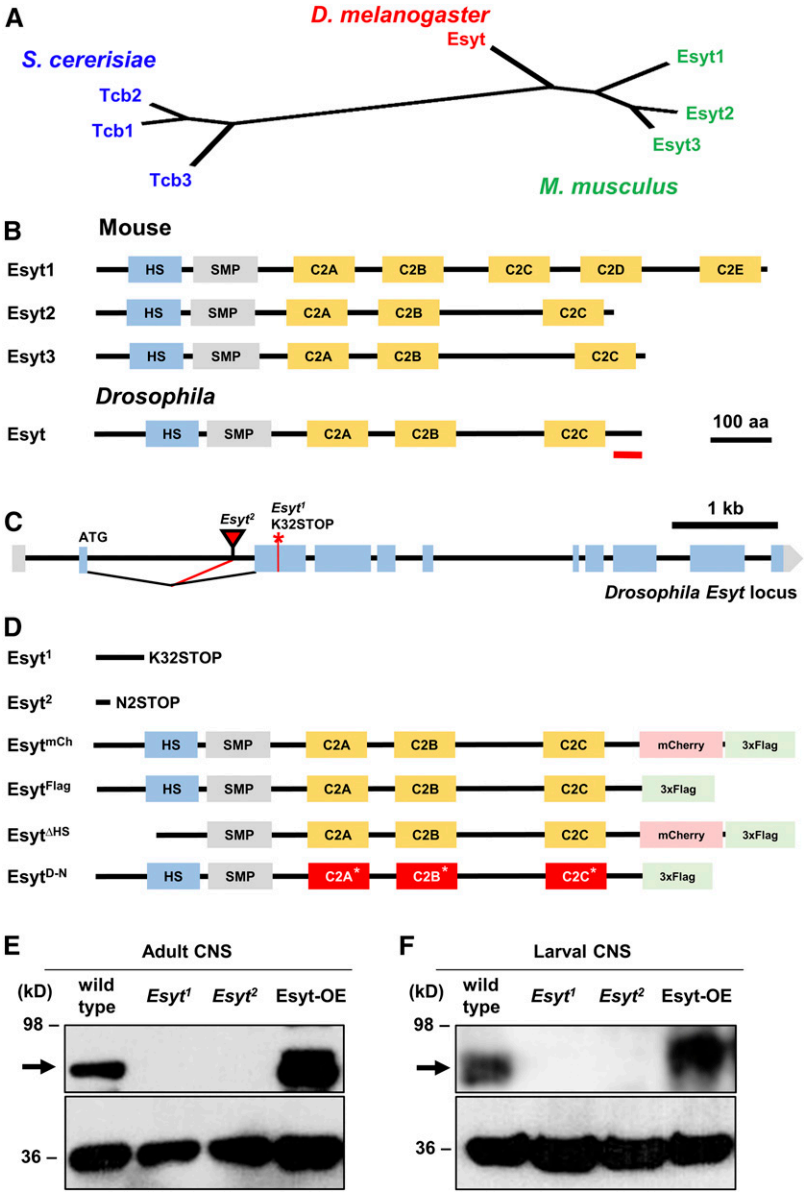

Figure 1 Genetic analysis and generation of null mutations in *Drosophila Esyt*. (A) Phylogenic analysis of the single *D. melanogaster Esyt* ortholog and the three *Esyt* genes encoded in *Mus musculus* (*Esyt1–3*) and *Saccharomyces cerevisiae* (*Tcb1–3*). (B) Schematic of the three Esyt protein structures aligned with the *Drosophila* homolog. The Esyt proteins contain an HS and an SMP, followed by multiple C_2 domains (C_2). Red line indicates the antigen against which the antibody was raised. (C) Schematic of the *Drosophila Esyt* locus. The CRISPR-induced early stop codon in *Esyt*^{1} (*) and the MiMIC transposon insertion site of *Esyt*^{2} (red triangle) are shown. *Esyt*^{1} and *Esyt*^{2} mutations are predicted to each truncate the open reading frame before the HS domain. (D) Schematic of *Esyt* mutations and engineered transgenes. For $Esyt_{D\text{-}N}$, C2 domains incapable of binding Ca^{2+} are indicated (*) and highlighted in red. Immunoblot analysis of Esyt expression in adult head lysates (E) and larval CNS lysates (F) demonstrates that *Esyt* is expressed in the nervous system and confirms both *Esyt*^{1} and *Esyt*^{2} alleles are protein nulls. The → indicates the expected molecular mass of Esyt. Neuronal overexpression of *Esyt* (Esyt-OE: *c155-Gal4;UAS-Esyt*^{Flag}) results in elevated levels and increased molecular mass for the tagged transgene, as expected. Anti-actin was used as loading control.

Drosophila Esyt is localized to presynaptic ER structures through the HS domain and that Ca^{2+} binding to Esyt appears to be required for Esyt trafficking in neurons.

Given that Esyt localizes to axonal ER, we examined the morphology of the ER network at synaptic terminals with loss or overexpression of *Esyt*. Expression of *GFP-KDEL* alone in motor neurons labeled an extensive presynaptic network throughout boutons, as observed by others (data not shown; Summerville *et al.* 2016). This network did not appear to be perturbed in *Esyt* mutants, nor with overexpression (data not shown). These results suggest that ER structure is not dependent on *Esyt* expression. Lastly, we found that the ER network labeled by Esyt is localized near, but distinct from, other synaptic compartments including active zones, synaptic vesicle pools, periactive zone regions, and the neuronal PM (Figure 2, E and F). Thus, Esyt is localized to the presynaptic ER network and present near areas of synaptic vesicle fusion and recycling at presynaptic terminals where it could, in principle, modulate synaptic structure and function.

Synaptic phospholipid balance does not require Esyt

Given that *Esyt* has been implicated in phospholipid transfer and homeostasis in nonneuronal cells, we next sought to determine whether the level or distribution of phospholipids at presynaptic terminals was altered in *Esyt* mutants and/or with overexpression of *Esyt* in motor neurons (Esyt-OE). The phospholipid phosphatidylinositol 4,5-bisphosphate [$PI(4,5)P_2$] plays crucial roles at presynaptic terminals, regulating synaptic protein–protein interactions, ion channel biophysics, neurotransmission, and synaptic vesicle trafficking (Ueda 2014; Lauwers *et al.* 2016). To measure synaptic levels of $PI(4,5)P_2$, we expressed a fluorescently tagged pleckstrin homology domain of phospholipase C-δ1 (PLCδ1-PH-GFP) that specifically labels $PI(4,5)P_2$ (Verstreken *et al.* 2009).

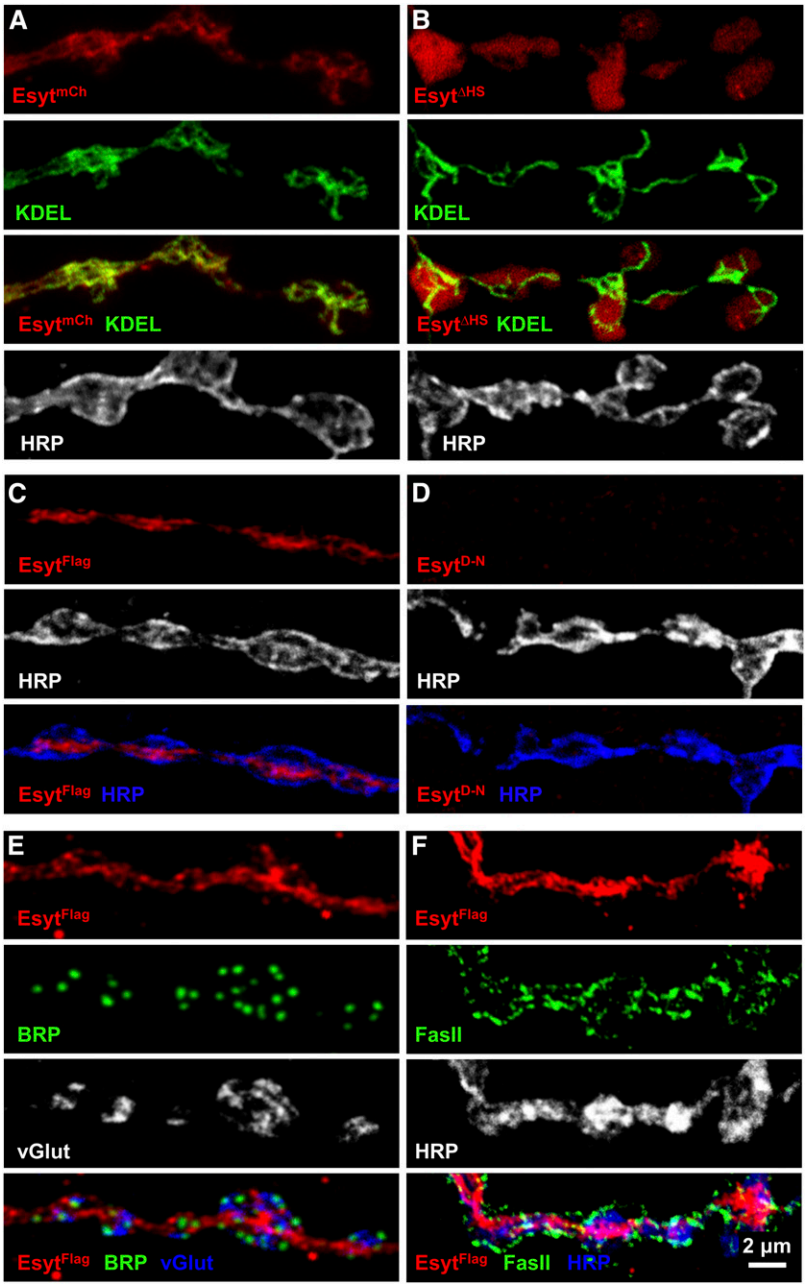

Figure 2 The HS is necessary to localize Esyt to axonal ER. (A) Representative images of third-instar larval NMJ with motor neuron expression of an mCherry-tagged *Esyt* transgene (Esyt^{mCh}; red) and a GFP-tagged ER marker (KDEL; green) (*w;OK6-Gal4/UAS-Esyt^{mCh};UAS-GFP-KDEL*), immunolabeled with the neuronal membrane marker HRP (white). Esyt^{mCh} colocalizes with axonal ER. (B) Deletion of the HS (*Esyt$^{\Delta HS}$*: *w;OK6-Gal4/UAS-Esyt$^{\Delta HS}$;UAS-GFP-KDEL*) results in a failure to localize to the ER, instead acquiring a cytosolic distribution. (C) Representative NMJ images of the Flag-tagged *Esyt* transgene (Esyt^{Flag}: anti-Flag; red) expressed in motor neurons (*w;OK6-Gal4/UAS-Esyt^{Flag}*) costained with HRP (white/blue). Esyt-Flag traffics to the presynaptic terminal and appears similar in distribution to Esyt^{mCh}. (D) Mutations in the *Esyt^{Flag}* transgene that prevent Ca^{2+} binding to C_2 domains (Esyt^{D-N}: *w;OK6-Gal4/UAS-Esyt^{D-N}*) no longer traffics to presynaptic terminals. (E) Axonal ER structures labeled with Esyt-Flag (anti-Flag; red) is shown relative to active zones (BRP; green) and synaptic vesicle structures (vGlut; white/blue). (F) Axonal ER labeled by Esyt-Flag (anti-Flag; red) is shown colabeled with a peri-active zone marker (FasII; green) and a neuronal membrane marker (HRP; white/blue).

Expression of this transgene in motor neurons revealed specific labeling of the PM at presynaptic terminals, consistent with the expected distribution of PI(4,5)P_2 (Figure 3A; Chen *et al.* 2014). When *PLCδ1-PH-GFP* was expressed in either *Esyt* mutants or Esyt-OE animals, we were unable to detect any difference in GFP intensity or distribution (Figure 3, A and B). Thus, we find no evidence that PI(4,5)P_2 levels or distribution is altered at synapses with gain or loss of *Esyt* expression.

In addition to the PM, the ER also associates with early and late endosomal structures, contributing to synaptic growth and vesicle trafficking (Rowland *et al.* 2014; Raiborg *et al.* 2015). Thus, we considered the possibility that Esyt may regulate lipid transfer or otherwise influence endosomes at synapses. We focused on early endosomes known to be involved in synaptic vesicle trafficking and recycling. These early endosomes are specifically labeled by the small GTPase Rab5 and are enriched in the phospholipid phosphatidylinositol-3-phosphate [PI(3)P] (Wucherpfennig *et al.* 2003). The FYVE finger domain of the Rab5 effectors EEA1 and Rabenosyin-5 bind specifically to PI(3)P, which is an established marker for early endosomes (Wucherpfennig *et al.* 2003). To test if PI(3)P levels and/or distribution are dependent on *Esyt* expression, we expressed a GFP-fused FYVE domain transgene (*GPF-myc-2xFYVE*) in *Esyt* mutants and Esyt-OE. *GFP-myc-2xFYVE* expression in controls labeled punctate structures in presynaptic boutons, as expected (Figure 3C). However, we observed no differences in the intensity of GFP-myc-2xFYVE

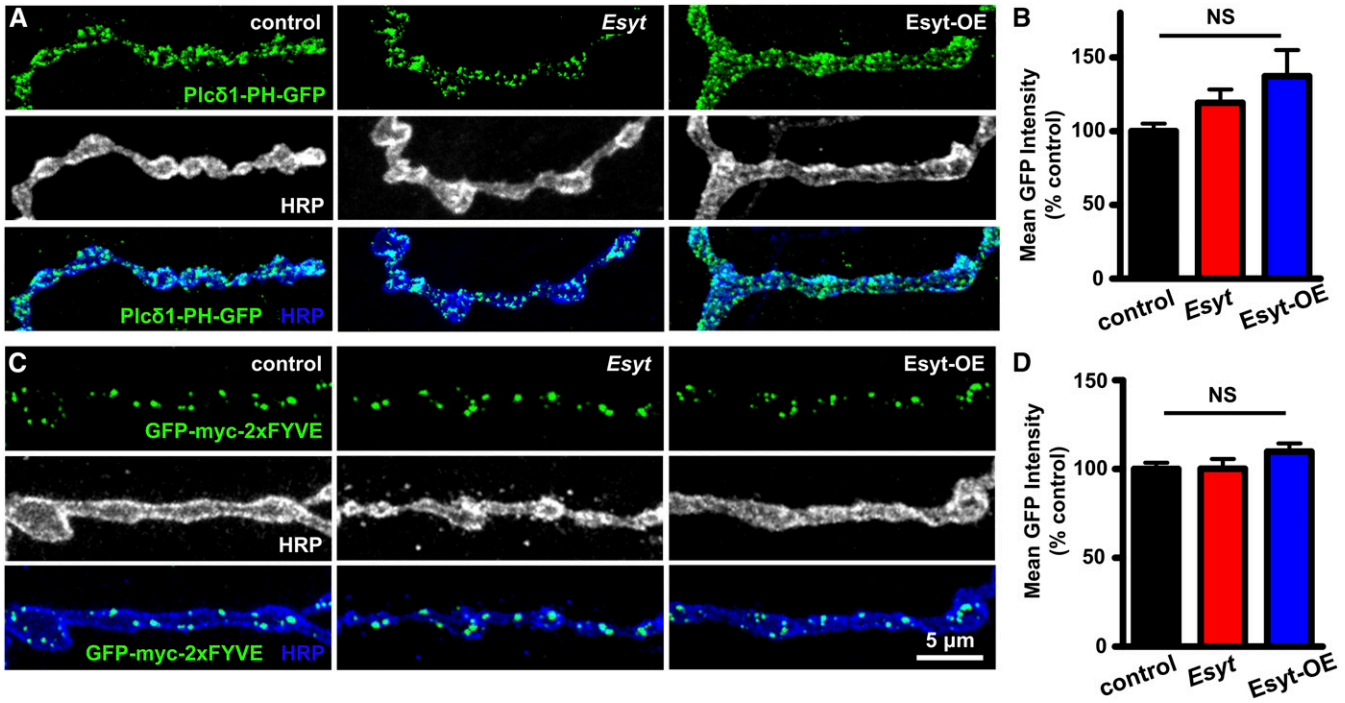

Figure 3 PI(4,5)P_2 and PI(3)P phospholipid levels are unchanged at presynaptic terminals in *Esyt* mutants and Esyt-OE. (A) Representative NMJ images of PI(4,5)P_2 labeled with PLCδ-PH-GFP (GFP; green) and HRP (white/blue) in control (*w;OK6-Gal4/+;UAS-PLCδ-PH-GFP/+*), *Esyt* mutants (*w;OK6-Gal4/+; Esyt*^{1}*/Esyt*^{2}*,UAS-PLCδ-PH-GFP*), and Esyt-OE (*w;OK6-Gal4/+; UAS-PLCδ1-PH-GFP/UAS-Esyt*^{Flag}). (B) Quantification of mean GFP intensity levels of the indicated genotypes. (C) Representative images of PI(3)P distribution at the NMJ labeled by GFP-myc-2xFYVE in control (*w;OK6-Gal4/UAS-GFP-myc-2xFYVE*), *Esyt* mutants (*w;OK6-Gal4/UAS-GFP-myc-2xFYVE;Esyt*^{1}*/Esyt*^{2}), and Esyt-OE (*w;OK6-Gal4/UAS-GFP-myc-2xFYVE;UAS-Esyt*^{Flag}*/+*). (D) Quantification of mean GFP intensity levels of the indicated genotypes. Error bars indicate ± SEM. One-way ANOVA test was performed, followed by a Tukey's multiple-comparison test. Detailed statistical information for represented data (mean values, SEM, *n*, *P*) is shown in Table S1. NS, not significant, $P > 0.05$.

in *Esyt* mutants and Esyt-OE compared to controls (Figure 3, C and D). Thus, we find no evidence that Esyt is involved in phospholipid balance, transfer, or distribution at presynaptic terminals.

Presynaptic overexpression of Esyt promotes synaptic growth

The axonal ER plays a critical role in synaptic growth and neurotransmission in mammals and *Drosophila* (Wong *et al.* 2014; Summerville *et al.* 2016; de Juan-Sanz *et al.* 2017). We therefore sought to determine to what extent *Esyt* expression contributes to synaptic development and neurotransmission. First, we quantified synaptic growth by immunostaining NMJs with antibodies that recognize neuronal membrane (HRP), active zones (BRP), and postsynaptic glutamate receptors (DGluRIII). *Esyt* mutants exhibited no significant differences in the number of synaptic boutons, nor in the number or density of active zones or glutamate receptor clusters at the NMJ (Figure 4, A–E). However, overexpression of the Esyt^{Flag} transgene in motor neurons revealed an ∼40% increase in synaptic growth, including increased neuronal membrane surface area and total number of active zones per NMJ (Figure 4, A–D), and similar results were observed when Esyt^{mCh} was overexpressed (Table S1). Thus, while loss of *Esyt* has no apparent impact on synaptic growth or structure, elevated levels of *Esyt* in motor neurons promotes synaptic growth at the NMJ.

Esyt has a role in facilitating presynaptic neurotransmitter release

The axonal ER is known to modulate presynaptic function (Wong *et al.* 2014; de Juan-Sanz *et al.* 2017), and we next assessed the impact on neurotransmission with loss or gain of *Esyt* expression. We recorded mEPSCs and EPSCs in low (0.4 mM) and high (3 mM) extracellular Ca^{2+} concentrations using a two-electrode voltage clamp configuration. We found no significant difference in mEPSC frequency or amplitude in *Esyt* mutants (Figure 5, A and B, and Table S1), consistent with no changes in the number of active zones or postsynaptic receptor clusters (Figure 4D). However, EPSC amplitude was reduced in *Esyt* mutants by >50% at low extracellular Ca^{2+}, with a concomitant decrease in quantal content compared to wild type (Figure 5, A–D). This reduction in EPSC amplitude and quantal content in *Esyt* mutants was also observed in high extracellular Ca^{2+} conditions, and rescued by expression of *Esyt* in motor neurons (Figure 5D and Table S1), demonstrating that presynaptic *Esyt* is necessary to promote neurotransmitter release. Indeed, there was an apparent shift in the Ca^{2+} sensitivity, but not cooperativity, of neurotransmission between wild type and *Esyt* mutants when

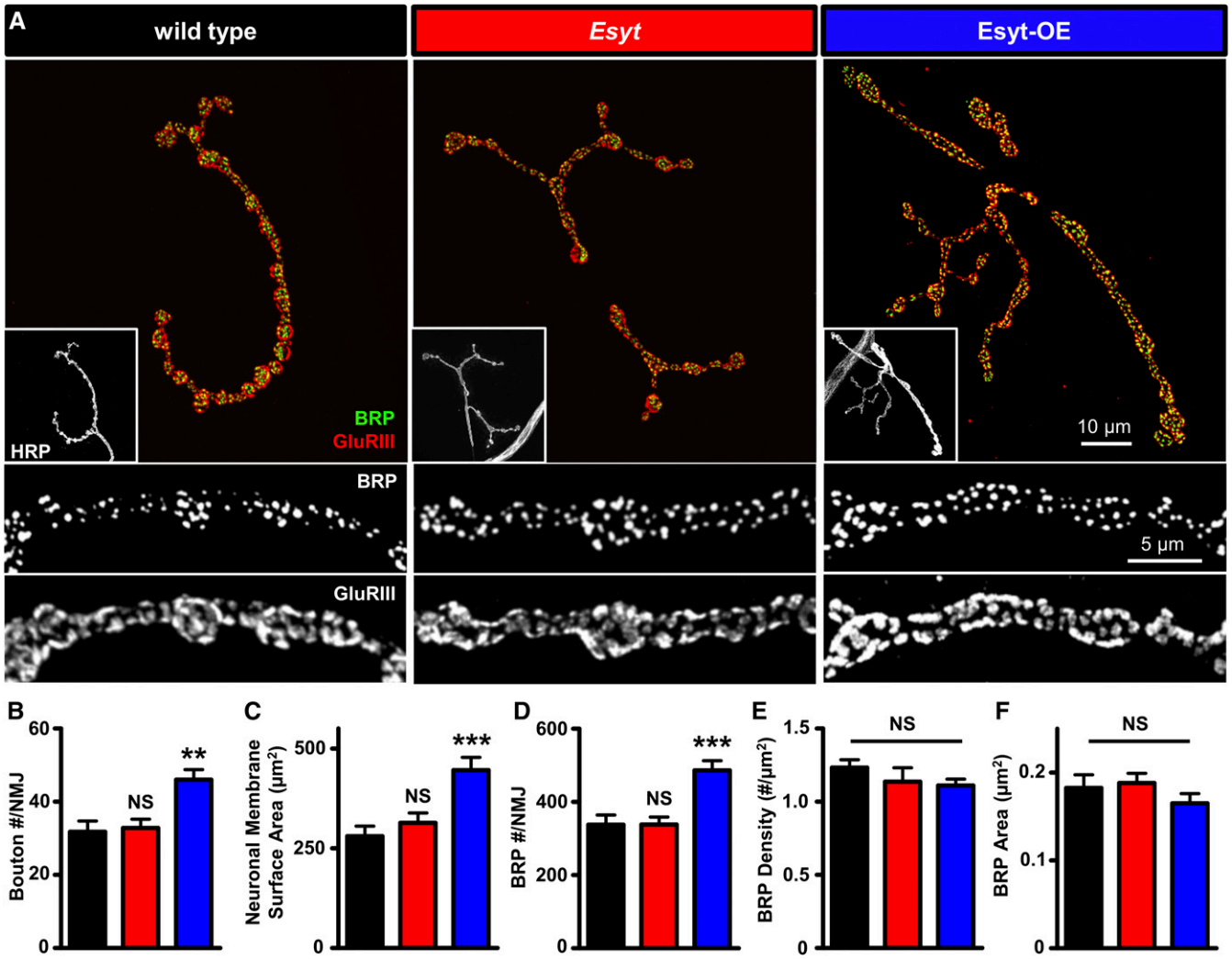

Figure 4 Presynaptic overexpression of *Esyt* promotes synaptic growth. (A) Representative NMJ images of wild type (w^{1118}), *Esyt* mutants (*Esyt*: $w;Esyt^{1}/Esyt^{2}$), and Esyt-OE ($w;OK6\text{-}Gal4/UAS\text{-}Esyt^{Flag}$) immunostained for anti-BRP (green), anti-GluRIII (red), and anti-HRP (white; inset). Bottom panels: BRP and GluRIII images at higher magnification. Quantification of bouton number per NMJ (B), neuronal membrane surface area (C), total BRP puncta number per NMJ (D), BRP density (E), and BRP area (F) of the indicated genotypes. Note that Esyt-OE results in increased bouton number and a corresponding increase in membrane and BRP number. Error bars indicate ± SEM. One-way ANOVA test was performed, followed by a Tukey's multiple-comparison test. Detailed statistical information for represented data (mean values, SEM, *n*, *P*) is shown in Table S1. NS, not significant, $P > 0.05$, ** $P \leq 0.01$, *** $P \leq 0.001$.

quantal content was assessed across a range of lowered extracellular Ca^{2+} concentrations (Figure 5D and Table S1). Thus, while *Esyt* mutants have no obvious defects in synaptic growth, Esyt is required for proper neurotransmission across a range of extracellular Ca^{2+} concentrations.

In contrast, we observed no significant differences in synaptic physiology at both low and elevated extracellular Ca^{2+} levels in Esyt-OE animals compared to controls (Figure 5, A–D and Table S1). Given the enhanced synaptic growth and active zone number in Esyt-OE, one may have expected a similarly enhanced degree of EPSC amplitude and quantal content, assuming no changes in release probability per active zone. This stable level of synaptic strength in Esyt-OE implies a reduction in release probability per active zone in Esyt-OE, an apparent homeostatic adaption (Davis and Muller 2015).

Finally, we probed short-term synaptic plasticity in *Esyt* mutants and Esyt-OE by evoking four stimuli at 60 Hz in low and high extracellular Ca^{2+}. Given that Esyt is a putative Ca^{2+} sensor localized to the axonal ER, this protocol would test a role for Esyt during rapid changes in presynaptic Ca^{2+} levels (Muller *et al.* 2011; Genç *et al.* 2017). At 0.4 mM extracellular Ca^{2+}, both wild-type and Esyt-OE animals showed moderate facilitation, with EPSC amplitudes finishing at ~150% of the starting EPSC amplitude (Figure 5, E and F). In contrast, *Esyt* mutants showed enhanced facilitation, with the last EPSC finishing at ~270% compared to the initial EPSC (Figure 5, E and F), consistent with reduced release probability in this condition. Similarly, at 3 mM extracellular Ca^{2+}, wild-type and Esyt-OE NMJs exhibited synaptic depression, with the fourth EPSC finishing at ~60% of the starting

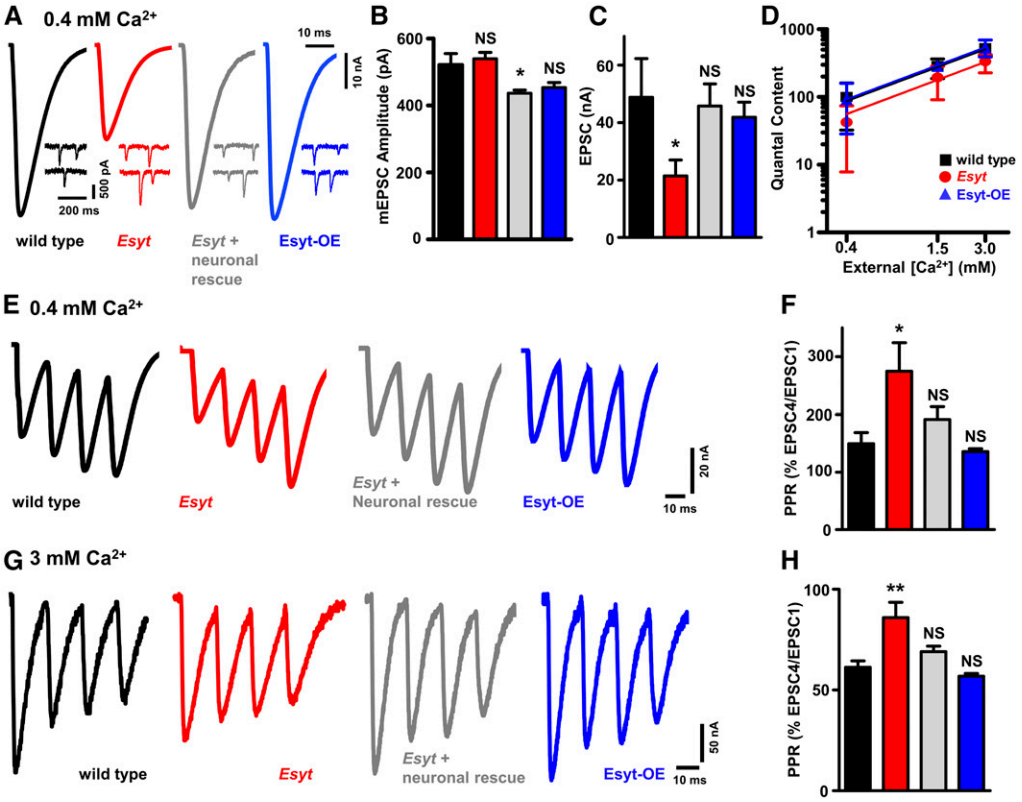

Figure 5 Esyt promotes presynaptic neurotransmitter release. (A) Representative electrophysiological EPSC and mEPSC traces for wild type, *Esyt* mutants, and Esyt-OE recorded in 0.4 mM extracellular Ca^{2+}. Quantification of mEPSC amplitude (B), EPSC amplitude (C), and quantal content plotted as a function of extracellular Ca^{2+} concentration on logarithmic scales (D) of the indicated genotypes. *Esyt* mutants exhibit significantly reduced synaptic transmission compared to wild type and Esyt-OE. No significant difference was observed in the slope of the best-fit lines used to determine the apparent Ca^{2+} cooperativity. Representative EPSC traces following four pulses of 60-Hz stimulation in wild type, *Esyt* mutants, *Esyt* neuronal rescue (*w*;*OK6-Gal4/UAS-Esyt*^{Flag}; *Esyt*^{1}/*Esyt*^{2}), and Esyt-OE in 0.4 mM (E) and 3 mM (G) extracellular Ca^{2+}. Quantification of average EPSC ratio (% fourth EPSC/first EPSC) for the indicated genotypes in 0.4 mM (F) and 3 mM (H) extracellular Ca^{2+}. *Esyt* mutants show reduced neurotransmission and short-term synaptic plasticity. Error bars indicate ± SEM. One-way ANOVA test was performed, followed by a Tukey's multiple-comparison test. Detailed statistical information for represented data (mean values, SEM, *n*, *P*) is shown in Table S1. NS, not significant, $P > 0.05$, * $P \leq 0.05$, ** P 0.01.

EPSC amplitude (Figure 5, G and H). Consistent with reduced release probability in this condition, *Esyt* mutants showed reduced depression, finishing at ~90% of the starting EPSC amplitude, which was rescued by presynaptic *Esyt* expression (Figure 5, G and H). Together, these data are consistent with a function for Esyt at the axonal ER in promoting synaptic vesicle release during evoked activity.

Esyt-OE synapses resist depletion during high-frequency stimulation

The axonal ER is involved in Ca^{2+} homeostasis at presynaptic terminals (Wong *et al.* 2014) and we considered that, during sustained levels of high activity, a role for Esyt in potentially regulating this process may be revealed. We therefore assessed synaptic transmission during elevated periods of activity in *Esyt* mutants and Esyt-OE. During high-frequency synaptic stimulation, endocytosis rates must be increased to sustain the elevated level of exocytosis, and any imbalance in this coupling will deplete the functional vesicle pool (Haucke *et al.* 2011). We used a previously established protocol in which we subject the fly NMJ to 10-Hz stimulation at elevated extracellular Ca^{2+} for 10 min, followed by recovery for an additional 10 min, taking a test pulse at 0.2 Hz (Verstreken *et al.* 2002; Dickman *et al.* 2005). This analysis revealed that wild-type and *Esyt*-mutant synapses exhibited a similar rate of vesicle pool depletion and recovery, finishing at ~30% of the original EPSP amplitude, followed by a recovery to ~60% of the initial value (Figure 6A). In both genotypes, a similar number of total quanta was released (Figure 6B). In contrast, Esyt-OE conferred a resistance to depletion and enhanced recovery of the functional synaptic vesicle pool. A 10-Hz stimulation of Esyt-OE NMJs revealed a slower rate of rundown and faster recovery of the depleted vesicle pool (Figure 6A), finishing at ~60% and recovering to ~90% of starting EPSP amplitudes. Indeed, more total quanta were released in Esyt-OE compared to both wild type and *Esyt* mutants during this sustained period of activity (Figure 6B). Together, this demonstrates that while the loss of *Esyt* does not significantly affect synaptic growth, structure, or vesicle recycling; overexpression of *Esyt* in neurons promotes synaptic growth which, while not affecting baseline transmission, appears to sustain the vesicle pool during prolonged activity.

The slowed rate of synaptic vesicle pool depletion in Esyt-OE could, in principle, be due to an increase in the number of synaptic vesicles participating in exocytosis and recycling at individual boutons. Alternatively, synaptic vesicle recycling at each bouton may be the same: the increased maintenance of the vesicle pool may be due to a reduced release probability per bouton coupled with the increased number of boutons in Esyt-OE, which are in effect, serving as a reservoir of additional vesicles available for release. We therefore examined NMJ ultrastructure to determine whether a change in the density of synaptic vesicles in each bouton was

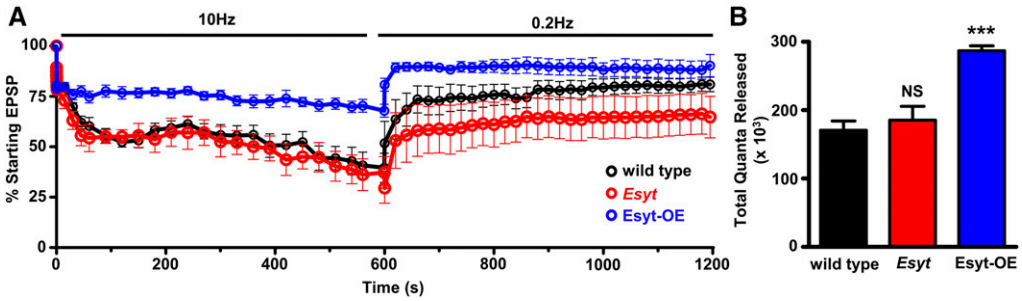

Figure 6 Esyt-OE synapses resist synaptic vesicle depletion during elevated activity. (A) Depletion and recovery of the functional vesicle pool in the indicated genotypes. NMJs were stimulated at 10 Hz for 10 min in 10 mM extracellular Ca^{2+}, then allowed to recover for 10 min while monitoring this recovery with stimulation at 0.2 Hz. EPSP amplitudes were averaged, normalized to prestimulus amplitudes, and plotted as a function of time. (B) Quantification of total quanta released during the 10 min of 10-Hz stimulation for the indicated genotypes. Error bars indicate ± SEM. One-way ANOVA test was performed, followed by a Tukey's multiple-comparison test. Detailed statistical information for represented data (mean values, SEM, n, p) is shown in Table S1. NS, not significant, $P > 0.05$, *** $P \leq 0.001$.

apparent, which may suggest an increased starting vesicle pool in Esyt-OE. We did not observe any significant change in the density or distribution of synaptic vesicles within NMJ boutons or near active zones in Esyt-OE compared with wild type and *Esyt* mutants (Figure 7, A–C). More generally, active zone length, T-bar morphology, and membrane compartments appear similar in all three genotypes (Figure 7, A–E). Thus, there is no evidence that Esyt-OE results in increased numbers or an altered distribution of synaptic vesicles within NMJ boutons.

Despite there being no change in the number of synaptic vesicles per bouton in Esyt-OE NMJs, it is possible that more synaptic vesicles participate in exo-endocytosis during activity which, in turn, could account for the increased maintenance of the functional vesicle pool. We therefore measured the pool of vesicles participating in endocytosis during high activity using the lipophilic dye FM1-43, which is absorbed by newly endocytosed synaptic vesicles from the PM following exocytosis and is a measure of the number of vesicles participating in release at each bouton (Dickman *et al.* 2005; Verstreken *et al.* 2008; Chen *et al.* 2014). Following stimulation, we observed a trend of reduced intensity of the vesicle pool labeled by FM1-43 in Esyt-OE compared to wild type and *Esyt* mutants (Figure 7, F and G), perhaps suggesting a reduction in the number of vesicles participating in exocytosis per bouton in Esyt-OE, consistent with reduced release probability per bouton. Thus, the increase in the total number of synaptic boutons, perhaps coupled with less vesicle release per bouton, likely accounts for the resistance to depletion of the vesicle pool in Esyt-OE during elevated activity.

Esyt is not required for presynaptic homeostatic potentiation

Thus far, we have found that *Esyt* has no apparent role in synaptic growth and structure, but is required to promote synaptic vesicle release across a range of extracellular Ca^{2+} concentrations. Interestingly, elevated Ca^{2+} influx at presynaptic terminals at the *Drosophila* NMJ has been demonstrated to drive an adaptive form of synaptic plasticity referred to presynaptic homeostatic potentiation (PHP) (Muller and Davis 2012; Davis and Muller 2015). At this synapse, pharmacological or genetic perturbations to postsynaptic glutamate receptors trigger a retrograde signal resulting in a precise increase in presynaptic neurotransmitter release, which compensates for reduced receptor functionality and restores synaptic strength to baseline levels (Frank 2014). Intriguingly, a recent study identified a multiple C_2 domain protein, called MCTP, which is anchored to the axonal ER and is necessary for PHP at the *Drosophila* NMJ (Genç *et al.* 2017). MCTP is structurally similar to Esyt, and we hypothesized that Esyt may also be an axonal ER C_2 domain protein that promotes vesicle release in response to homeostatic signaling. Application of the glutamate receptor antagonist PhTx-433 (Frank *et al.* 2006) to wild-type NMJs led to the expected ~50% reduction in mEPSP amplitude but normal EPSP amplitude because of a homeostatic increase in quantal content (presynaptic release) (Figure 8). Similarly, PhTx reduced mEPSP amplitudes in both *Esyt* mutants and Esyt-OE, and both genotypes exhibited a robust increase in quantal content (Figure 8). Thus, loss or increased expression of *Esyt* has no consequence for the acute induction or expression of PHP.

Discussion

We have generated the first mutations in the single *Drosophila Esyt* ortholog and characterized the presynaptic localization and functions of this gene at the NMJ. We demonstrate that *Drosophila* Esyt is localized to an extensive axonal ER network. Although Esyt was previously shown to mediate ER–PM tethering and to promote lipid exchange between the two membranes in nonneuronal cells, we find no evidence that lipid balance is altered at *Esyt* mutant synapses. While there is no apparent change in synaptic growth or structure in *Esyt* mutants, we find that *Esyt* is required to facilitate presynaptic release across a range of extracellular Ca^{2+}. Interestingly, presynaptic overexpression of *Esyt* promotes synaptic growth and, in turn, resistance to synaptic depression during elevated activity. Together, our study establishes Esyt as a conserved ER-localized protein that regulates neurotransmission and synaptic growth when overexpressed.

Esyt localizes to the axonal ER and promotes neurotransmission

Given the high conservation of the *Esyt* family throughout evolution and its function in Ca^{2+}-dependent lipid transfer,

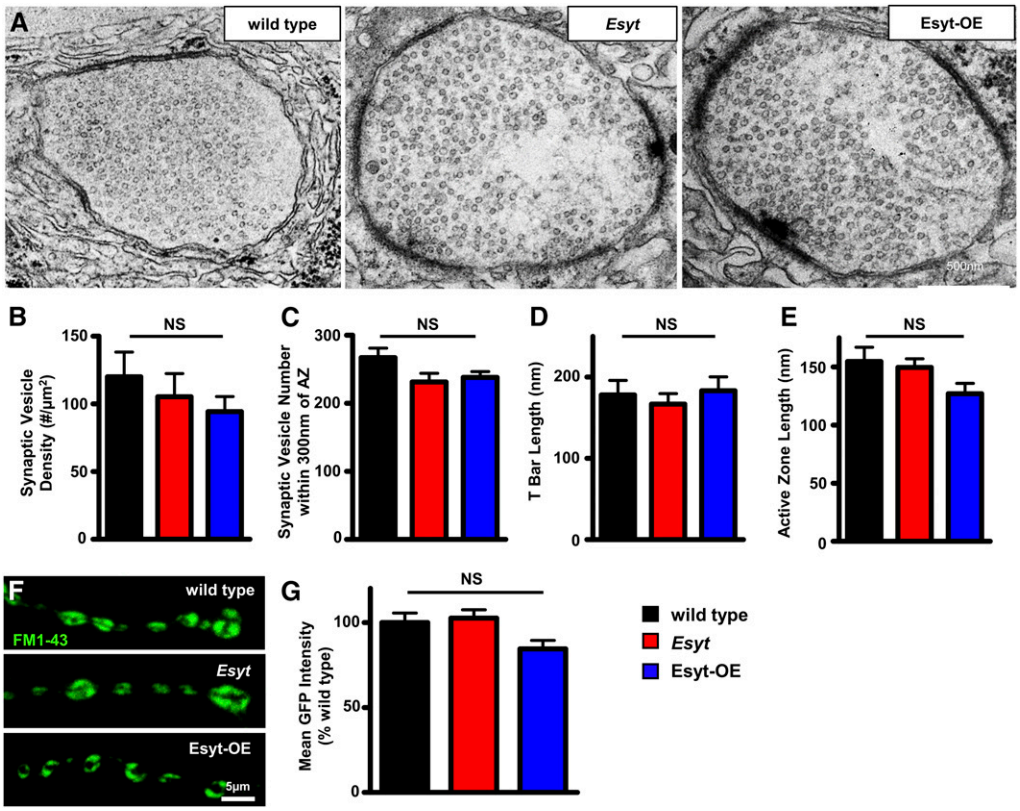

Figure 7 Synaptic vesicle density and endocytic pools are unchanged in *Esyt* mutants and Esyt-OE. (A) Representative electron micrograph images of NMJs for wild type, *Esyt* mutants, and Esyt-OE. Quantification of synaptic vesicle density (B), synaptic vesicles within 300 nm of the active zone (C), T-bar length (D), and active zone length (E) in the indicated genotypes. No significant differences were observed. (F) Representative images of FM1-43 dye loading of the indicated genotypes. (G) Quantification of mean intensity of the FM1-43 signal in the indicated genotypes. Error bars indicate ± SEM. One-way ANOVA test was performed, followed by a Tukey's multiple-comparison test. Detailed statistical information for represented data (mean values, SEM, *n*, *P*) is shown in Table S1. NS, not significant, $P > 0.05$.

Esyt was an attractive candidate to play a role in modulating lipid metabolism at synapses. Accordingly, we find that Esyt is localized to the axonal ER. However, we find that Esyt is not required to maintain lipid homeostasis at synapses, at least for the major phospholipids PI(4,5)P_2 and PI(3)P. This demonstrates that lipid balance and membrane homeostasis can be maintained during the extreme demands of regulated membrane trafficking and exchange at presynaptic terminals in the absence of *Esyt*. In retrospect, this may not be surprising as a lipid cycle nested within the synaptic vesicle cycle has long been known to exist at synapses, and this is supported by key synaptic proteins such as Synaptojanin, Rab5, Minibrain kinase/Dyrk1A, and Sac1 (De Camilli *et al.* 1996; Nemoto *et al.* 2000; Wenk and De Camilli 2004; Chen *et al.* 2014). Importantly, there is no known involvement or requirement for acute lipid transfer from the ER in synaptic vesicle recycling (De Camilli *et al.* 1996; Wenk and De Camilli 2004). Accordingly, lipid homeostasis during synaptic vesicle trafficking, like protein homeostasis, may be sufficiently embedded and coupled in membrane trafficking itself so as not to lead to imbalances, even during rapid synaptic vesicle exo- and endocytosis.

Despite no apparent changes in synaptic lipid metabolism in *Esyt* mutants, these animals demonstrated a significant reduction in EPSC amplitude across a range of extracellular Ca^{2+} conditions. This finding suggests that Esyt may promote presynaptic function by coupling local Ca^{2+} dynamics to axonal ER Ca^{2+} release. Indeed, the axonal ER has emerged as a crucial organelle that can sense and dynamically respond to changes in cytosolic Ca^{2+} to modulate presynaptic function

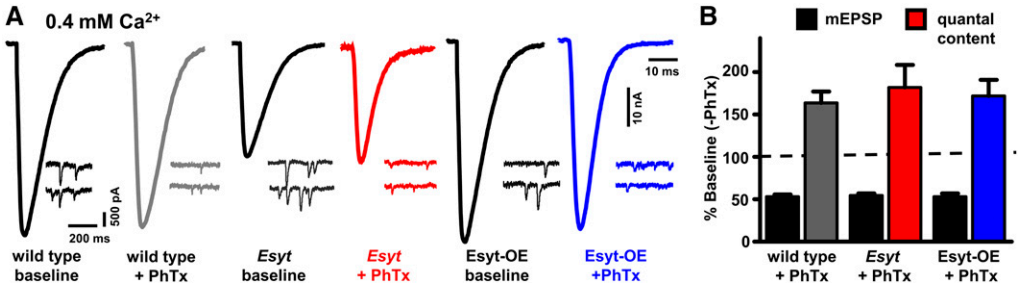

Figure 8 *Esyt* is dispensable for presynaptic homeostatic plasticity. (A) Representative EPSC and mEPSC traces for wild type, *Esyt* mutants, and Esyt-OE before (baseline) and following PhTx application. Note that while mEPSC amplitudes are reduced following PhTx application, EPSC amplitudes recover to baseline levels because of a homeostatic increase in presynaptic release (quantal content). (B) Quantification of mEPSC and quantal content values after PhTx application normalized to baseline values. No significant differences were observed. Error bars indicate ± SEM. One-way ANOVA test was performed, followed by a Tukey's multiple-comparison test. Detailed statistical information for represented data (mean values, SEM, *n*, *P*) is shown in Table S1.

and plasticity (Verkhratsky 2005; Bardo *et al.* 2006; Kwon *et al.* 2016; de Juan-Sanz *et al.* 2017). For example, Ca^{2+} influx from the extracellular space can induce additional Ca^{2+} release from the ER via ryanodine receptors, a process referred as Ca^{2+}-induced Ca^{2+} release (CICR), which can be activated during single action potentials or trains of stimuli (Verkhratsky 2005; Bardo *et al.* 2006; Kwon *et al.* 2016; de Juan-Sanz *et al.* 2017). An intriguing possibility is that Esyt may work in conjunction with ryanodine receptors as Ca^{2+} sensors that promote CICR at the presynaptic terminal in response to activity. In this model, Esyt may respond to elevated Ca^{2+} at synapses during single action potentials, leading to a supplemental source of presynaptic Ca^{2+}, perhaps through release of intracellular ER stores (Scott *et al.* 2008).

Esyt, axonal ER, and synaptic growth

Perhaps the most striking and unexpected finding was that elevated expression of *Esyt* in motor neurons led to increased synaptic growth and enhanced resistance to synaptic depression. To our knowledge, genes encoding proteins with multiple C_2 domains and an HS, such as Esyt, MCTP, and Ferlins, have not been associated with synaptic growth (Lek *et al.* 2012; Genç *et al.* 2017). We consider two possible mechanisms for how overexpression of Esyt may promote synaptic growth. First, Esyt may modulate intracellular Ca^{2+} levels at synapses, which have been shown to play a role in regulating synaptic growth at the *Drosophila* NMJ. Indeed, the TRPV channel inactive (Iav) is present on axonal ER and modulates synaptic growth by regulating Ca^{2+} release from ER stores, which signals through calcineurin to stabilize microtubules (Wong *et al.* 2014). Although loss of *Esyt* does not appear to affect synaptic growth, further studies will be necessary to determine whether elevated levels of Esyt alters ER Ca^{2+} release or resting Ca^{2+} levels, perhaps by interacting with factors such as Iav.

Another attractive possibility is that elevated *Esyt* expression at the axonal ER may promote increased membrane trafficking from the ER to the PM at synapses through the constitutive pathway. Indeed, the membrane necessary for synaptic growth is delivered through this pathway, as synapses are established and continue to grow and elaborate even when toxins that block or inhibit synaptic vesicle fusion are expressed (Broadie *et al.* 1995; Sweeney *et al.* 1995; Dickman *et al.* 2006; Choi *et al.* 2014). Facilitated delivery of synaptic proteins and membrane to the presynaptic terminal, in turn, may lead to excess membrane and fuel-increased synaptic growth. Further, inhibition of axonal ER export during early developmental stages results in defective axon growth in mouse hippocampal neurons (Aridor and Fish 2009). Thus, the unanticipated finding that increased *Esyt* expression promotes synaptic growth raises the intriguing possibility that synaptic proteins and membrane derived from the axonal ER may be a rate-limiting step in driving synapse expansion.

We have established Esyt as an axonal ER protein that promotes presynaptic function and may also have unanticipated roles in regulating synaptic growth. Future studies using approaches such as Ca^{2+} imaging will be necessary to elucidate the molecular mechanisms of how Esyt modulates axonal ER activity to ultimately promote neurotransmission. Further genetic experiments will likely reveal additional insights into how excess Esyt levels at synapses enhance synaptic growth, perhaps through interactions with other axonal ER proteins that control Ca^{2+} release from ER stores, such as Iav. Although the axonal ER was first observed >40 years ago (Tsukita and Ishikawa 1976; Ramirez and Couve 2011), the functions of this complex organelle have remained enigmatic. Recent studies have begun to reveal how the axonal ER sculpts presynaptic Ca^{2+} dynamics and modulates presynaptic function and plasticity (de Juan-Sanz *et al.* 2017), roles that seem certain to contribute to a variety of neurological diseases.

Acknowledgments

We acknowledge the Developmental Studies Hybridoma Bank (Iowa City, IA) for antibodies and the Bloomington *Drosophila* Stock Center for fly stocks. We also thank Christopher Buser at Droseran LLC (Pasadena, CA) for technical assistance with electron microscopy. This work was supported in part by a University of Southern California Provost Fellowship to K.K. and by a National Institutes of Health grant to D.K.D. (NS-091546), as well as funding from the Alfred P. Sloan, Ellison Medical, Mallinckrodt, Whitehall, and Klingenstein–Simons Foundations to D.K.D. The authors declare no competing financial interests.

Author contributions: K.K. and D.K.D. conceived the project and designed the research. K.K., X.L., D.K., and D.S. performed experiments. K.K., X.L., D.K., and D.S. analyzed data. K.K. and D.K.D. wrote the manuscript.

Literature Cited

Aberle, H., A. P. Haghighi, R. D. Fetter, B. D. McCabe, T. R. Magalhaes *et al.*, 2002 Wishful thinking encodes a BMP type II receptor that regulates synaptic growth in Drosophila. Neuron 33: 545–558.

Aridor, M., and K. N. Fish, 2009 Selective targeting of ER exit sites supports axon development. Traffic 10: 1669–1684.

Atwood, H. L., C. K. Govind, and C. F. Wu, 1993 Differential ultrastructure of synaptic terminals on ventral longitudinal abdominal muscles in Drosophila larvae. J. Neurobiol. 24: 1008–1024.

Bardo, S., M. G. Cavazzini, and N. Emptage, 2006 The role of the endoplasmic reticulum Ca2+ store in the plasticity of central neurons. Trends Pharmacol. Sci. 27: 78–84.

Berger, C., H. Harzer, T. R. Burkard, J. Steinmann, S. van der Horst *et al.*, 2012 FACS purification and transcriptome analysis of drosophila neural stem cells reveals a role for Klumpfuss in self-renewal. Cell Rep. 2: 407–418.

Bischof, J., R. K. Maeda, M. Hediger, F. Karch, and K. Basler, 2007 An optimized transgenesis system for Drosophila using germ-line-specific phiC31 integrases. Proc. Natl. Acad. Sci. USA 104: 3312–3317.

Blackstone, C., C. J. O'Kane, and E. Reid, 2011 Hereditary spastic paraplegias: membrane traffic and the motor pathway. Nat. Rev. Neurosci. 12: 31–42.

Broadie, K., A. Prokop, H. J. Bellen, C. J. O'Kane, K. L. Schulze *et al.*, 1995 Syntaxin and synaptobrevin function downstream of vesicle docking in Drosophila. Neuron 15: 663–673.

Budnik, V., Y. H. Koh, B. Guan, B. Hartmann, C. Hough *et al.*, 1996 Regulation of synapse structure and function by the Drosophila tumor suppressor gene dlg. Neuron 17: 627–640.

Chakroborty, S., I. Goussakov, M. B. Miller, and G. E. Stutzmann, 2009 Deviant ryanodine receptor-mediated calcium release resets synaptic homeostasis in presymptomatic 3xTg-AD mice. J. Neurosci. 29: 9458–9470.

Chang, C. L., and J. Liou, 2016 Homeostatic regulation of the PI (4,5)P2-Ca(2+) signaling system at ER-PM junctions. Biochim. Biophys. Acta 1861: 862–873.

Chen, C. K., C. Bregere, J. Paluch, J. F. Lu, D. K. Dickman *et al.*, 2014 Activity-dependent facilitation of synaptojanin and synaptic vesicle recycling by the Minibrain kinase. Nat. Commun. 5: 4246.

Chen, X., W. Ma, S. Zhang, J. Paluch, W. Guo *et al.*, 2017 The BLOC-1 subunit pallidin facilitates activity-dependent synaptic vesicle recycling. eNeuro 4: ENEURO.0335-16.2017.

Cheung, K. H., D. Shineman, M. Muller, C. Cardenas, L. Mei *et al.*, 2008 Mechanism of Ca2+ disruption in Alzheimer's disease by presenilin regulation of InsP3 receptor channel gating. Neuron 58: 871–883.

Choi, B. J., W. L. Imlach, W. Jiao, V. Wolfram, Y. Wu *et al.*, 2014 Miniature neurotransmission regulates Drosophila synaptic structural maturation. Neuron 82: 618–634.

Daines, B., H. Wang, L. Wang, Y. Li, Y. Han *et al.*, 2011 The Drosophila melanogaster transcriptome by paired-end RNA sequencing. Genome Res. 21: 315–324.

Davis, G. W., and M. Muller, 2015 Homeostatic control of presynaptic neurotransmitter release. Annu. Rev. Physiol. 77: 251–270.

De Camilli, P., S. D. Emr, P. S. McPherson, and P. Novick, 1996 Phosphoinositides as regulators in membrane traffic. Science 271: 1533–1539.

de Juan-Sanz, J., G. T. Holt, E. R. Schreiter, F. de Juan, D. S. Kim *et al.*, 2017 Axonal endoplasmic reticulum Ca2+ content controls release probability in CNS nerve terminals. Neuron 93: 867–881.e6.

Deng, M., W. He, Y. Tan, H. Han, X. Hu *et al.*, 2013 Increased expression of reticulon 3 in neurons leads to reduced axonal transport of beta site amyloid precursor protein-cleaving enzyme 1. J. Biol. Chem. 288: 30236–30245.

Deshpande, M., and A. A. Rodal, 2016 The crossroads of synaptic growth signaling, membrane traffic and neurological disease: insights from Drosophila. Traffic 17: 87–101.

Dickman, D. K., and G. W. Davis, 2009 The schizophrenia susceptibility gene dysbindin controls synaptic homeostasis. Science 326: 1127–1130.

Dickman, D. K., J. A. Horne, I. A. Meinertzhagen, and T. L. Schwarz, 2005 A slowed classical pathway rather than kiss-and-run mediates endocytosis at synapses lacking synaptojanin and endophilin. Cell 123: 521–533.

Dickman, D. K., Z. Lu, I. A. Meinertzhagen, and T. L. Schwarz, 2006 Altered synaptic development and active zone spacing in endocytosis mutants. Curr. Biol. 16: 591–598.

Dong, B., K. Kakihara, T. Otani, H. Wada, and S. Hayashi, 2013 Rab9 and retromer regulate retrograde trafficking of luminal protein required for epithelial tube length control. Nat. Commun. 4: 1358.

Fasana, E., M. Fossati, A. Ruggiano, S. Brambillasca, C. C. Hoogenraad *et al.*, 2010 A VAPB mutant linked to amyotrophic lateral sclerosis generates a novel form of organized smooth endoplasmic reticulum. FASEB J. 24: 1419–1430.

Frank, C. A., 2014 Homeostatic plasticity at the Drosophila neuromuscular junction. Neuropharmacology 78: 63–74.

Frank, C. A., M. J. Kennedy, C. P. Goold, K. W. Marek, and G. W. Davis, 2006 Mechanisms underlying the rapid induction and sustained expression of synaptic homeostasis. Neuron 52: 663–677.

Genç, Ö., D. K. Dickman, W. Ma, A. Tong, R. D. Fetter *et al.*, 2017 MCTP is an ER-resident calcium sensor that stabilizes synaptic transmission and homeostatic plasticity. Elife 6: e22904.

Giordano, F., Y. Saheki, O. Idevall-Hagren, S. F. Colombo, M. Pirruccello *et al.*, 2013 PI(4,5)P(2)-dependent and Ca(2+)-regulated ER-PM interactions mediated by the extended synaptotagmins. Cell 153: 1494–1509.

Goussakov, I., M. B. Miller, and G. E. Stutzmann, 2010 NMDA-mediated Ca(2+) influx drives aberrant ryanodine receptor activation in dendrites of young Alzheimer's disease mice. J. Neurosci. 30: 12128–12137.

Gratz, S. J., A. M. Cummings, J. N. Nguyen, D. C. Hamm, L. K. Donohue *et al.*, 2013 Genome engineering of Drosophila with the CRISPR RNA-guided Cas9 nuclease. Genetics 194: 1029–1035.

Graveley, B. R., A. N. Brooks, J. W. Carlson, M. O. Duff, J. M. Landolin *et al.*, 2011 The developmental transcriptome of Drosophila melanogaster. Nature 471: 473–479.

Guindon, S., J. F. Dufayard, V. Lefort, M. Anisimova, W. Hordijk *et al.*, 2010 New algorithms and methods to estimate maximum-likelihood phylogenies: assessing the performance of PhyML 3.0. Syst. Biol. 59: 307–321.

Han, C., L. Y. Jan, and Y. N. Jan, 2011 Enhancer-driven membrane markers for analysis of nonautonomous mechanisms reveal neuron-glia interactions in Drosophila. Proc. Natl. Acad. Sci. USA 108: 9673–9678.

Haucke, V., E. Neher, and S. J. Sigrist, 2011 Protein scaffolds in the coupling of synaptic exocytosis and endocytosis. Nat. Rev. Neurosci. 12: 127–138.

Herdman, C., and T. Moss, 2016 Extended-synaptotagmins (E-Syts); the extended story. Pharmacol. Res. 107: 48–56.

Idevall-Hagren, O., A. Lu, B. Xie, and P. De Camilli, 2015 Triggered Ca2+ influx is required for extended synaptotagmin 1-induced ER-plasma membrane tethering. EMBO J. 34: 2291–2305.

Jean, S., A. Mikryukov, M. G. Tremblay, J. Baril, F. Guillou *et al.*, 2010 Extended-synaptotagmin-2 mediates FGF receptor endocytosis and ERK activation in vivo. Dev. Cell 19: 426–439.

Jean, S., M. G. Tremblay, C. Herdman, F. Guillou, and T. Moss, 2012 The endocytic adapter E-Syt2 recruits the p21 GTPase activated kinase PAK1 to mediate actin dynamics and FGF signalling. Biol. Open 1: 731–738.

Khuong, T. M., R. L. Habets, J. R. Slabbaert, and P. Verstreken, 2010 WASP is activated by phosphatidylinositol-4,5-bisphosphate to restrict synapse growth in a pathway parallel to bone morphogenetic protein signaling. Proc. Natl. Acad. Sci. USA 107: 17379–17384.

Kiragasi, B., J. Wondolowski, Y. Li, and D. K. Dickman, 2017 A presynaptic glutamate receptor subunit confers robustness to neurotransmission and homeostatic potentiation. Cell Rep. 19: 2694–2706.

Kwon, S. K., Y. Hirabayashi, and F. Polleux, 2016 Organelle-specific sensors for monitoring Ca2+ dynamics in neurons. Front. Synaptic Neurosci. 8: 29.

Lauwers, E., R. Goodchild, and P. Verstreken, 2016 Membrane lipids in presynaptic function and disease. Neuron 90: 11–25.

Lek, A., F. J. Evesson, R. B. Sutton, K. N. North, and S. T. Cooper, 2012 Ferlins: regulators of vesicle fusion for auditory neurotransmission, receptor trafficking and membrane repair. Traffic 13: 185–194.

Mackler, J. M., J. A. Drummond, C. A. Loewen, I. M. Robinson, and N. E. Reist, 2002 The C(2)B Ca(2+)-binding motif of synaptotagmin is required for synaptic transmission in vivo. Nature 418: 340–344.

Manford, A. G., C. J. Stefan, H. L. Yuan, J. A. Macgurn, and S. D. Emr, 2012 ER-to-plasma membrane tethering proteins regulate cell signaling and ER morphology. Dev. Cell 23: 1129–1140.

Marrus, S. B., S. L. Portman, M. J. Allen, K. G. Moffat, and A. DiAntonio, 2004 Differential localization of glutamate receptor

subunits at the Drosophila neuromuscular junction. J. Neurosci. 24: 1406–1415.
Min, S. W., W. P. Chang, and T. C. Sudhof, 2007 E-Syts, a family of membranous Ca2+-sensor proteins with multiple C2 domains. Proc. Natl. Acad. Sci. USA 104: 3823–3828.
Montenegro, G., A. P. Rebelo, J. Connell, R. Allison, C. Babalini *et al.*, 2012 Mutations in the ER-shaping protein reticulon 2 cause the axon-degenerative disorder hereditary spastic paraplegia type 12. J. Clin. Invest. 122: 538–544.
Muller, M., and G. W. Davis, 2012 Transsynaptic control of presynaptic Ca(2)(+) influx achieves homeostatic potentiation of neurotransmitter release. Curr. Biol. 22: 1102–1108.
Muller, M., E. C. Pym, A. Tong, and G. W. Davis, 2011 Rab3-GAP controls the progression of synaptic homeostasis at a late stage of vesicle release. Neuron 69: 749–762.
Nagarkar-Jaiswal, S., P.-T. Lee, M. E. Campbell, K. Chen, S. Anguiano-Zarate *et al.*, 2015 A library of MiMICs allows tagging of genes and reversible, spatial and temporal knockdown of proteins in Drosophila. eLife 4: e05338.
Nandi, N., L. K. Tyra, D. Stenesen, and H. Kramer, 2014 Acinus integrates AKT1 and subapoptotic caspase activities to regulate basal autophagy. J. Cell Biol. 207: 253–268.
Nemoto, Y., B. G. Kearns, M. R. Wenk, H. Chen, K. Mori *et al.*, 2000 Functional characterization of a mammalian Sac1 and mutants exhibiting substrate-specific defects in phosphoinositide phosphatase activity. J. Biol. Chem. 275: 34293–34305.
Noreau, A., P. A. Dion, and G. A. Rouleau, 2014 Molecular aspects of hereditary spastic paraplegia. Exp. Cell Res. 325: 18–26.
Okajima, T., B. Reddy, T. Matsuda, and K. D. Irvine, 2008 Contributions of chaperone and glycosyltransferase activities of O-fucosyltransferase 1 to Notch signaling. BMC Biol. 6: 1.
Pfenninger, K. H., 2009 Plasma membrane expansion: a neuron's Herculean task. Nat. Rev. Neurosci. 10: 251–261.
Raiborg, C., E. M. Wenzel, N. M. Pedersen, H. Olsvik, K. O. Schink *et al.*, 2015 Repeated ER-endosome contacts promote endosome translocation and neurite outgrowth. Nature 520: 234–238.
Ramirez, O. A., and A. Couve, 2011 The endoplasmic reticulum and protein trafficking in dendrites and axons. Trends Cell Biol. 21: 219–227.
Renvoisé, B., and C. Blackstone, 2010 Emerging themes of ER organization in the development and maintenance of axons. Curr. Opin. Neurobiol. 20: 531–537.
Rowland, A. A., P. J. Chitwood, M. J. Phillips, and G. K. Voeltz, 2014 ER contact sites define the position and timing of endosome fission. Cell 159: 1027–1041.
Saheki, Y., and P. De Camilli, 2017 The extended-synaptotagmins. Biochim. Biophys. Acta 1864: 1490–1493.
Saheki, Y., X. Bian, C. M. Schauder, Y. Sawaki, M. A. Surma *et al.*, 2016 Control of plasma membrane lipid homeostasis by the extended synaptotagmins. Nat. Cell Biol. 18: 504–515.
Sclip, A., T. Bacaj, L. R. Giam, and T. C. Sudhof, 2016 Extended synaptotagmin (ESyt) triple knock-out mice are viable and fertile without obvious endoplasmic reticulum dysfunction. PLoS One 11: e0158295.
Scott, R., T. Lalic, D. M. Kullmann, M. Capogna, and D. A. Rusakov, 2008 Target-cell specificity of kainate autoreceptor and Ca2+-store-dependent short-term plasticity at hippocampal mossy fiber synapses. J. Neurosci. 28: 13139–13149.
Stewart, B. A., H. L. Atwood, J. J. Renger, J. Wang, and C. F. Wu, 1994 Improved stability of Drosophila larval neuromuscular preparations in haemolymph-like physiological solutions. J. Comp. Physiol. A 175: 179–191.
Summerville, J. B., J. F. Faust, E. Fan, D. Pendin, A. Daga *et al.*, 2016 The effects of ER morphology on synaptic structure and function in Drosophila melanogaster. J. Cell Sci. 129: 1635–1648.
Sweeney, S. T., K. Broadie, J. Keane, H. Niemann, and C. J. O'Kane, 1995 Targeted expression of tetanus toxin light chain in Drosophila specifically eliminates synaptic transmission and causes behavioral defects. Neuron 14: 341–351.
Teuling, E., S. Ahmed, E. Haasdijk, J. Demmers, M. O. Steinmetz *et al.*, 2007 Motor neuron disease-associated mutant vesicle-associated membrane protein-associated protein (VAP) B recruits wild-type VAPs into endoplasmic reticulum-derived tubular aggregates. J. Neurosci. 27: 9801–9815.
Tremblay, M. G., C. Herdman, F. Guillou, P. K. Mishra, J. Baril *et al.*, 2015 Extended synaptotagmin interaction with the fibroblast growth factor receptor depends on receptor conformation, not catalytic activity. J. Biol. Chem. 290: 16142–16156.
Tsukita, S., and H. Ishikawa, 1976 Three-dimensional distribution of smooth endoplasmic reticulum in myelinated axons. J. Electron Microsc. (Tokyo) 25: 141–149.
Ueda, Y., 2014 The role of phosphoinositides in synapse function. Mol. Neurobiol. 50: 821–838.
Venken, K. J., K. L. Schulze, N. A. Haelterman, H. Pan, Y. He *et al.*, 2011 MiMIC: a highly versatile transposon insertion resource for engineering Drosophila melanogaster genes. Nat. Methods 8: 737–743.
Verkhratsky, A., 2005 Physiology and pathophysiology of the calcium store in the endoplasmic reticulum of neurons. Physiol. Rev. 85: 201–279.
Verstreken, P., O. Kjaerulff, T. E. Lloyd, R. Atkinson, Y. Zhou *et al.*, 2002 Endophilin mutations block clathrin-mediated endocytosis but not neurotransmitter release. Cell 109: 101–112.
Verstreken, P., T. Ohyama, and H. J. Bellen, 2008 FM 1–43 labeling of synaptic vesicle pools at the Drosophila neuromuscular junction. Methods Mol. Biol. 440: 349–369.
Verstreken, P., T. Ohyama, C. Haueter, R. L. Habets, Y. Q. Lin *et al.*, 2009 Tweek, an evolutionarily conserved protein, is required for synaptic vesicle recycling. Neuron 63: 203–215.
Wenk, M. R., and P. De Camilli, 2004 Protein-lipid interactions and phosphoinositide metabolism in membrane traffic: insights from vesicle recycling in nerve terminals. Proc. Natl. Acad. Sci. USA 101: 8262–8269.
Wong, C. O., K. Chen, Y. Q. Lin, Y. Chao, L. Duraine *et al.*, 2014 A TRPV channel in Drosophila motor neurons regulates presynaptic resting Ca2+ levels, synapse growth, and synaptic transmission. Neuron 84: 764–777.
Wucherpfennig, T., M. Wilsch-Brauninger, and M. Gonzalez-Gaitan, 2003 Role of Drosophila Rab5 during endosomal trafficking at the synapse and evoked neurotransmitter release. J. Cell Biol. 161: 609–624.
Yang, Y. S., N. Y. Harel, and S. M. Strittmatter, 2009 Reticulon-4A (Nogo-A) redistributes protein disulfide isomerase to protect mice from SOD1-dependent amyotrophic lateral sclerosis. J. Neurosci. 29: 13850–13859.
Yu, H., Y. Liu, D. R. Gulbranson, A. Paine, S. S. Rathore *et al.*, 2016 Extended synaptotagmins are Ca2+-dependent lipid transfer proteins at membrane contact sites. Proc. Natl. Acad. Sci. USA 113: 4362–4367.
Zhang, C., B. Wu, V. Beglopoulos, M. Wines-Samuelson, D. Zhang *et al.*, 2009 Presenilins are essential for regulating neurotransmitter release. Nature 460: 632–636.

Communicating editor: H. Bellen